Optimizing $Al_xGa_{1-x}N$ separate confinement heterostructure lasers with large band discontinuities

Pankaj Shah and Vladimir Mitin[a)]
Electrical and Computer Engineering Department, Wayne State University, Detroit, Michigan 48202

(Received 30 September 1996; accepted for publication 29 January 1997)

Two-dimensional simulations were performed to optimize the waveguiding region's aluminum composition of an AlGaN/GaN separate confinement heterostructure (SCH) laser with large band discontinuities. Results demonstrate that the active region's thickness, waveguiding regions' thickness, and the material composition of the waveguiding region should be optimized, based on losses of the materials in the structure. Results also demonstrate that the threshold current of a SCH laser may be larger than that of a double heterostructure laser. The increase is caused by a competition between the active region and the waveguiding region which has a parasitic effect on the laser's modal gain because of the waveguiding region's slightly larger band gap, so that below the lasing threshold, photon emission and population inversion can occur in both regions. At the minimum threshold current the structure is optimized to strongly confine both the guided optical mode and the charge carriers responsible for the gain. © *1997 American Institute of Physics.* [S0021-8979(97)08609-X]

INTRODUCTION

There have recently been several successful demonstrations of current injection pumped, nitride based semiconductor lasers.[1–3] Lasers based on alloys of AlN, GaN, and InN are desirable because light emission would be possible over a continuous range from red through the ultraviolet portion of the optical spectrum with the high end portion of this frequency range dominated by AlGaN. One important benefit of this is the higher density of information that can be stored using shorter wavelength light. However, the greatest roadblock in the creation of these lasers at this early stage is the development of the growth technology. To enhance this research activity, there have been many theoretical calculations of the current flow behavior, optical gain, and lasing threshold currents in nitride based semiconductor laser structures.[4–9] However, to our knowledge, numerical simulations which take into account the energy band structure, spectral characteristics of recombination and gain, current spreading and optical mode waveguiding in a consistent manner to give results as close to reality as possible, have only been done for nitride based light emitting diodes[5] and double heterostructure lasers.[8] Simulations of devices with wide energy gaps are much more difficult than narrow energy gap devices because the carrier concentrations present at certain locations in the device make the equations involved ill-conditioned, thwarting the solution procedure. However, simulations are important to learn how the currently available materials are expected to perform, and how the device can be optimized to overcome some of the disadvantages introduced by thepoor material quality. Using simulations we have alreadydemonstrated that the threshold current of an $Al_{0.4}Ga_{0.6}N/GaN/Al_{0.4}Ga_{0.6}N$ double heterostructure (DH) laser can be minimized by optimizing the active region thickness and that in very lossy materials it is best to avoid very thin active region structures.[8]

The AlGaN material system is being actively investigated for the fabrication of current injection pumped lasers, though as of yet, experimental results have only been published for optically pumped stimulated emission in a vertical cavity laser structure,[10] a double heterostructure laser,[11] and a separate confinement heterostructure (SCH) laser.[12] For most applications the SCH is expected to give the best performance. As is well known, the threshold current density can be minimized, by optimizing at separate locations, the energy barriers for charge carrier flow, and the refractive index difference between the waveguiding and cladding layers. This is the idea behind the SCH design. However, numerical simulations of this are necessary to truly understand what effect the combination of effective masses, refractive indexes, affinities, and energy band gaps available in this material system have on the threshold current, in the SCH structure. We have now performed the first numerical simulation of the nitride based SCH semiconductor laser structure, to demonstrate how the threshold current changes with the Al composition of the waveguiding regions, the thicknesses of the active and waveguiding regions, and the losses present in the active region. We have investigated the performance of $Al_{0.4}Ga_{0.6}N/Al_xGa_{1-x}N/GaN/Al_xGa_{1-x}N/Al_{0.4}Ga_{0.6}N$ separate confinement heterostructure lasers in which GaN is the active region, for different Al composition in the waveguiding regions, $Al_xGa_{1-x}N$.

The structure investigated here is in line with current growth capabilities. Though most AlGaN based devices have an Al composition of 0.15 or less, higher amounts have been used. For instance, the vertical cavity SCH structure mentioned above contained Bragg reflectors made from $Al_{0.4}Ga_{0.6}N$, and $Al_xGa_{1-x}N$ has been grown with an aluminum composition, x, ranging from 0 up to 1.0.[13]

We have observed the threshold current for lasing sharply increases, then gradually decreases and passes through a minimum and finally increases again, as the waveguiding regions' aluminum composition increases from

[a)]Electronic mail: mitin@ece6.eng.wayne.edu

 0021-8979/97/81(9)/5930/5/$10.00

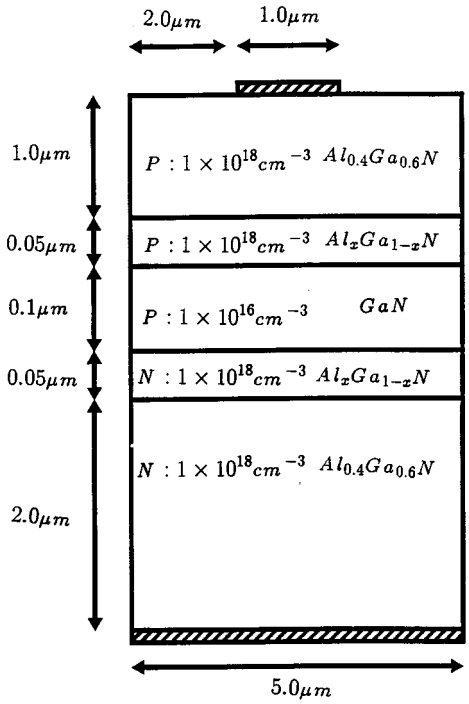

FIG. 1. The simulated separate confinement heterostructure laser which contains a GaN active region, $Al_xGa_{1-x}N$ waveguiding regions, and $Al_{0.4}Ga_{0.6}N$ cladding layers.

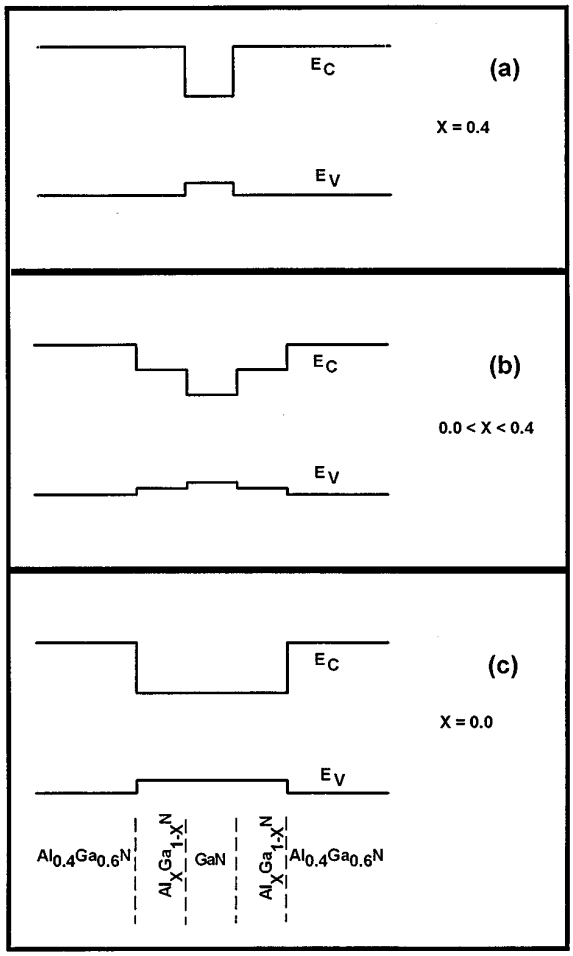

FIG. 2. Diagram of the energy band structure taken along a vertical cut through the center of Fig. 1, to demonstrate the location of band discontinuities. In (a), the waveguiding region consists of $Al_{0.4}Ga_{0.6}N$, in (b) the waveguiding region's composition, x, is between 0.0 and 0.4. In (c), the waveguiding designated region is composed of GaN. E_C is the conduction band and E_V is the valence band.

near zero. The increase near $x = 0$ is significant, and to our knowledge, it was not presented in the literature yet. Because the growth technology for these materials is not very advanced, the materials fabricated today have very high optical losses. The results presented here demonstrate that the waveguiding region's aluminum composition for minimum threshold current is dependent on the quality of the available material. Also, these results indicate that it may not be best to use very low values of x in the waveguiding regions of SCH lasers.

DEVICE STRUCTURE AND SIMULATION PROCEDURE

Figure 1 presents the structure, dimensions, and dopant concentrations of the SCH laser under investigation. It has a GaN active region, $Al_xGa_{1-x}N$ waveguiding regions, and $Al_{0.4}Ga_{0.6}N$ cladding layers. For most of the discussions presented here, a structure with a 0.1 μm thick active region was investigated because this thickness is associated with the minimum threshold current density in a DH laser made from $Al_{0.4}Ga_{0.6}N$/GaN/$Al_{0.4}Ga_{0.6}N$ with a GaN active region, as observed in earlier simulations.[8] Using this structure, we demonstrate that further optimization is possible by introducing the waveguiding regions with proper material composition. At the end of this article, results for a thinner active region structure (0.06 μm) are presented to validate the observations, and present trends. The optical mode's intensity at the peak is largest in the DH laser with a waveguide thickness of 0.2 μm. Therefore, the total thickness of the SCH's waveguide was set to 0.2 μm. The total structure's width was set to 5 μm, and the top electrode's width to only 1 μm. These two values were chosen because of the strong interest in wide band-gap lasers for optical disc recorders, where self-sustained pulsations (SSPs) provides a practical method for reducing noise. To induce SSP, enough saturable absorption is needed in the active region, which is more likely to occur in narrow stripe lasers.[14] Fortunately, these narrower stripe structures will also produce much higher modal gain in AlGaN lasers, compared to AlGaAs lasers, because the injected current does not spread as much in the low mobility nitride semiconductors. Figure 2 presents a diagram of the energy band structure along a vertical cut through the center of Fig. 1, for lasers with different waveguiding region compositions to indicate the location of energy barriers present in the different structures considered here. Figure 2(a) presents the band structure when the waveguiding region consists of $Al_{0.4}Ga_{0.6}N$, Fig. 2(b) presents the same when the waveguiding regions consists of $Al_xGa_{1-x}N$ with $0.0<x<0.4$, and Fig. 2(c) presents the same for the case when the waveguiding designated regions consist of GaN.

For the simulation results presented here, we have solved Poisson's equation, the electron and hole continuity equations and the wave equation for the electromagnetic

TABLE I. Material parameters of AlN and GaN.

Parameter	AlN	Reference	GaN	Reference	Units
m_e^*	$0.48m_0$	16	$0.2m_0$	17	⋯
m_h^*	$0.7m_0$	estimate	$0.4m_0$	18	⋯
μ_n	300	16	600	19	$cm^2/V/s$
μ_p	14	20	9	21	$cm^2/V/s$
$\epsilon_r(0)$	8.5	22	9.0	22	⋯
$\epsilon_r(\infty)$	4.7	22	5.35	22	⋯
Ref. index	2.15	22	2.67	22	⋯
Direct energy gap	6.2	23	3.43	24	eV
Electron affinity	7.64	25	10.23	25	eV
Spin orbit splitting	12	26	11	27	meV

field of the emitted light, self-consistently over the two-dimensional cross section of the structure. Thermionic emission of charge carriers at the heterojunctions, was included in the simulations. The spontaneous recombination rate and gain are calculated by integrating the electron and hole distributions in the energy bands of the device according to formulas derived from Fermi's golden rule and assuming that the k-selection rule holds.[15] The lasing threshold is reached when the modal gain equals the optical losses present, with single mode lasing assumed. For optical losses, two values were chosen. First, the limiting case where only mirror losses are present in a laser with a cavity length of 100 μm ($\alpha=157\ cm^{-1}$). Second, we assumed total losses roughly twice the limiting value ($\alpha=300\ cm^{-1}$) to see the influence of losses on the lasing threshold current. This was done to observe trends as the material's losses decrease, which will occur as the growth technology improves. Parameter values for AlN and GaN, used in the simulations, are as listed in Table I. Parameter values for the alloy AlGaN were obtained by taking corresponding proportions of the values for the constituent compounds.

RESULTS AND DISCUSSIONS

With $x=0.4$, which is at the high end of the range investigated here [see Fig. 2(a)], this structure corresponds to an $Al_{0.4}Ga_{0.6}N/GaN/Al_{0.4}Ga_{0.6}N$ DH laser. This structure's active region's thickness is the optimum value as presented in Ref. 8, for the lowest threshold current density, when the total optical losses, are due to only mirror losses. With this as a starting point, the aluminum composition of the now defined waveguiding regions are reduced for further optimization. With large x in the waveguiding regions, charge carriers build up in the active region due to two reasons. First, the recombination rate is small in the structure because the region with the lowest energy gap has a short extent in the direction of the current flow, which reduces the time that charge carriers interact to recombine there. Second, the large band discontinuity at the heterojunction between the cladding layer and the waveguiding layer minimizes the leakage of charge carriers out of the central regions by thermionic emission. With the resulting charge carrier buildup in the active region, the gain spectrum is broad.

As x decreases [see Fig. 2(b)] in the SCH structure investigated here, to define separate regions for waveguiding and charge carrier confinement, the performance of the laser improves. The buildup of charge carrier concentrations is reduced in the active region due to a decrease in the barrier's height, which they have to surmount, to leave the active region by thermionic emission. This barrier now consists of two smaller steps rather than one large step. At the same time, the peak of the modal gain spectra is higher for a fixed amount of current injection because the optical mode confinement improves as x decreases. The modal gain spectrum presents a weighted product of the material gain and the local photon density which is determined by the optical mode confinement. The stronger modal gain spectrum leads to increased stimulated emission which also reduces the charge carrier buildup. In turn, the modal gain spectrum becomes narrower. Since less charge carrier buildup occurs, additional charge carriers injected into the thin active region recombine quicker, since they are at much lower energy levels in their respective bands, i.e., the quasi-Fermi levels are closer to the energy band edges.

Eventually an optimal x is reached, where the optical confinement is strong enough and the injection and confinement of charge carriers efficient enough to give the minimum threshold current density.

As x is further reduced [approaching the structure shown in Fig 2(c)] the waveguiding regions' energy gap narrows and in turn, the material gain increases there, due to the inverse dependence of material gain on the emitted photon's energy in a particular region. Also, for small enough x, the energy barriers between the active region and the waveguiding regions are small and charge carriers will build up in both regions. Thus, there is a buildup of gain in the active region and a parasitic buildup in the waveguiding regions. A single region with a uniform energy gap will have a modal gain spectra consisting of a single peak, and the spectral shape will be determined by material parameters and the electron and hole distributions, assuming single-mode lasing. Because the three central regions of the SCH laser investigated here have different energy gaps, their individual contributions to the modal gain spectra can lead to two peaks. Lasing can occur first at the energy associated with the peak having higher gain. This in turn determines the threshold current density. The gain spectra for the parasitic region have a strong contribution, over a fraction of its energy range from charge carriers that can recombine in the active region. In an improperly designed structure, the modal gain could be highest in this energy range rather than the energy range associated with light emission due to stimulated emission only from the active region. Even in a properly designed structure, if the pumping level is very high, the gain of the active and waveguiding regions may both reach the lasing threshold, and then lasing at two frequencies will occur.

Figure 3 demonstrates the positions of the quasi-Fermi levels for electrons, E_{FN}, and holes, E_{FP}. These quasi-Fermi levels indicate the charge carrier distributions in the structure at the lasing threshold in both the active region and the waveguiding regions, for the structure with $x=0.02$ in the waveguiding regions, and assuming that the total optical losses are $\alpha=300\ cm^{-1}$. This figure clearly shows that the separation of the quasi-Fermi levels is larger than the energy

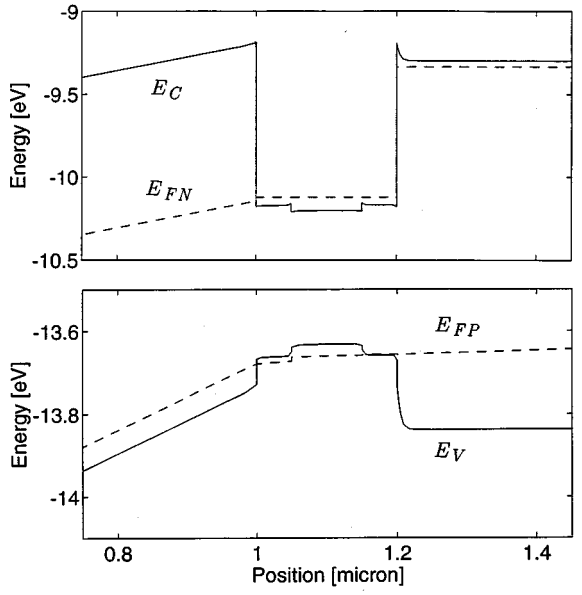

FIG. 3. Band structure at lasing threshold, along a vertical cut through the center of the structure in Fig. 1. The waveguiding regions are composed of $Al_{0.02}Ga_{0.98}N$. E_C is the conduction band, E_V is the valence band, E_{FN} is the electron quasi-Fermi level, and E_{FP} is the hole quasi-Fermi level. Please note that the energy axes are scaled differently for the valence and conduction bands.

gap, in both the active and the waveguiding regions, which is necessary for gain.

When the aluminum concentration of the waveguiding regions, x, is very close to zero, charge carrier confinement to the active region is poor, and this structure behaves like a double heterojunction laser with a 0.2 μm thick active region [see Fig. 2(c) for a band diagram of the structure]. Whether charge carriers are in the active region or in the regions designated as the waveguiding region, they will contribute almost equally to the laser gain. The modal gain will be weak because of poor overlap between the inverted population of charge carriers and the guided photons.

To clarify the ideas of this section, Fig. 4 presents the calculated gain spectra at lasing threshold, for an AlGaN SCH laser with total optical losses of $\alpha = 300\ \mathrm{cm}^{-1}$, when the waveguiding layers' aluminum composition is $x=0.3$, $x=0.1$, $x=0.02$, and $x=0.005$. The two separate humps in the gain spectra for $x=0.02$ are due to the competition to reach the threshold, between the waveguiding and active regions. One of these humps is due to the population inversion in the active region, and the second corresponds mainly to the waveguiding region with a contribution from the active region. For the $x = 0.005$ case the gain spectrum is narrower because a smaller range of energy levels are filled by charge carriers compared to the cases represented by the other curves. These spectra are narrower even though the threshold current is higher because the large number of charge carriers that contribute to population inversion and material gain, do not encounter enough photons to produce stimulated emission, due to the presence of strong waveguiding but weak charge carrier confinement. These gain curves also indicate a shift in the wavelength of emitted light as the aluminum composition of the waveguiding regions increases.

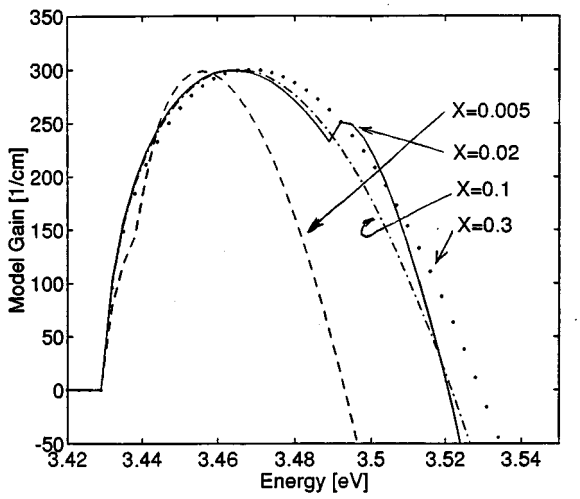

FIG. 4. The modal gain spectra, at the lasing threshold, for structures containing waveguiding regions composed of $Al_xGa_{1-x}N$ with $x=0.005$, $x=0.02$, $x=0.1$, and $x = 0.03$. Total optical losses are 300 cm^{-1}.

The gain spectra indicate how the injected carriers fill the active region, and the carrier injection necessary for the device to reach the lasing threshold. The plot of the threshold current versus aluminum composition, x, in the waveguiding region, as shown in Fig. 5, demonstrates this behavior in a different fashion. The solid curves in this figure are for the structure with a 0.1 μm thick active region. Represented are structures with total optical losses of $\alpha = 157\ \mathrm{cm}^{-1}$, for which the maximum threshold current occurs at $x=0.01$, and for $\alpha = 300\ \mathrm{cm}^{-1}$, in which case the maximum occurs at $x=0.02$. As x increases from zero, the threshold current density increases due to the independent pumping of the active region and the parasiticlike waveguiding regions, as men-

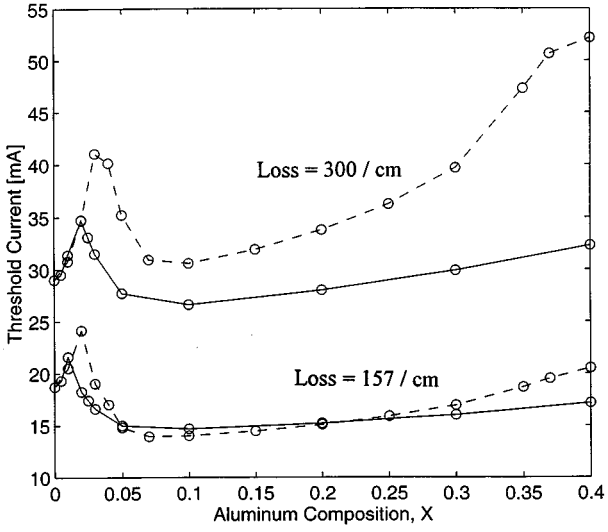

FIG. 5. Dependence of the lasing threshold current on aluminum composition, x, in the waveguiding regions. The two lower curves are for total optical losses of 157 cm^{-1} and the two upper curves are for total optical losses of 300 cm^{-1}. The solid lines represent the case of a 0.1 μm thick active region, and the dashed lines represent the case of a 0.06 μm thick active region. In both cases the active region is centered in the waveguiding region, and the waveguiding region's total thickness is 0.2 μm.

tioned above. The threshold current decreases to a minimum, as demonstrated in Fig. 5, as x approaches 0.1 because a balance is reached between the strong confinement of the guided mode due to the refractive index difference between waveguiding and cladding regions, and the strong confinement of charge carriers due to the large energy barriers around the active region. For $x > 0.1$ the threshold current increases again because the gain spectra broadens and the optical confinement, which determines the modal gain, reduces.

The shift of the peaks in Fig. 5, to higher x values, as the total losses increase, is due to charge carrier buildup in both the waveguiding and the active regions of the laser, when it is pumped more intensely, to reach the gain necessary for lasing at higher losses. This buildup broadens the gain spectra which changes the energy of the maximum gain, and in turn the location of the peak in the threshold current density versus composition plot.

A similar plot was calculated for a laser structure with a thinner active region but with an overall waveguiding region thickness still just 0.2 μm, to further confirm these results and observe trends. The dashed line in Fig. 5, represents the case where the active region is centered vertically in the waveguide region as before, but now has a thickness of only 0.06 μm. The material composition and other dimensions are the same as before. The peak near low x values is higher and wider for this case because now the volume of the region that has a parasitic effect on the gain is greater so more injected carriers are wasted in creating a population inversion in this region. From Fig. 5, we observe that at low losses, the minimum of the threshold current is lower than when the active region was 0.1 μm thick. However, as the losses increase, for the narrower active region structure, the optimal waveguiding region's composition changes from $x=0.07$ to $x=0$. These effects are due to the interplay between the optical confinement and charge carrier confinement.

The values calculated here for threshold can be compared to the measurement of the threshold of optically pumped stimulated emission of $\approx 90\ \mathrm{kW/cm^2}$.[12] Let us assume that every electron injected into the 0.1 μm active region would add to the population inversion and could recombine to produce one photon at a lasing energy of 3.47 eV which is near the peak of the gain spectra for the $x=0.02$, $x=0.1$, and $x=0.3$ cases, as shown in Fig. 4. Assuming very little lateral spreading occurs of charge carriers flowing from the top contact to the active region allows one to choose a 1 μm wide active region. In this case, the optimal injected current of 26.5 mA, which is near the minimum of the solid curve in Fig. 5, provides the same amount of population inversion, for the lasing threshold, as an optical pumping power of $920\ \mathrm{W/cm^2}$, assuming that the total losses are 300 $\mathrm{cm^{-1}}$. A stronger comparison is not possible because the actual aluminum compositions of the different regions of the structure in Ref. 12, as well as the total losses, are not known.

CONCLUSION

Two-dimensional numerical simulation results are presented, for an AlGaN separate confinement heterostructure laser with a GaN active region, demonstrating that besides optimizing the width of the active region, the composition of the waveguiding regions should be optimized. These results also indicate that with an improper waveguiding region's composition, the threshold current may be higher than in a double heterostructure laser, when the waveguiding regions have very low aluminum composition. Furthermore, these results demonstrate that the material's total optical losses have a strong influence on the optimum material composition for the waveguiding regions.

ACKNOWLEDGMENT

This work was supported by a grant from the Army Research Office.

[1] S. Nakamura, M. Senoh, S. Nagahama, N. Iwasa, T. Yamada, T. Matsushita, H. Kiyoku, and Y. Sugimoto, Jpn. J. Appl. Phys. 1 **35**, L217 (1996).
[2] I. Akasaki, S. Sota, H. Sakai, T. Tanaka, M. Koike, and H. Amano, Electron. Lett. **32**, 1105 (1996).
[3] S. Nakamura, M. Senoh, S. Nagahama, N. Iwasa, and T. Yamada, Appl. Phys. Lett. **68**, 3269 (1996).
[4] A. T. Meney, E. P. O'Reilly, and A. R. Adams, Semicond. Sci. Technol. **11**, 897 (1996).
[5] P. Shah, V. Mitin, K. Hess, M. Grupen, and G. H. Song, J. Appl. Phys. **79**, 2755 (1996).
[6] P. Rees, C. Cooper, P. M. Smowton, P. Blood, and J. Hegarty, IEEE Photonics Technol. Lett. **8**, 197 (1996).
[7] W. W. Chow, A. F. Wright, and J. S. Nelson, Appl. Phys. Lett. **68**, 296 (1996).
[8] P. Shah and V. Mitin, IEEE Trans. Electron. Devices (to be published).
[9] W. Fang and S. L. Chuang, Appl. Phys. Lett. **67**, 751 (1995).
[10] J. M. Redwing, D. A. S. Loeber, N. G. Anderson, M. A. Tischler, and J. S. Flynn, Appl. Phys. Lett. **69**, 1 (1996).
[11] R. L. Aggarwal, P. A. Maki, R. J. Molnar, Z. L. Liau, and I. Melngailis, J. Appl. Phys. **79**, 2148 (1996).
[12] T. J. Schmidt, X. H. Yang, W. Shan, J. J. Song, A. Salvador, W. Kim, O. Aktas, A. Botchkarev, and H. Morkoç, Appl. Phys. Lett. **68**, 1820 (1996).
[13] S. Yoshida, S. Misawa, and S. Gonda, J. Appl. Phys. **53**, 6844 (1982).
[14] M. Yuri, J. S. Harris, Jr., T. Takayama, O. Imafuji, H. Naito, M. Kume, K. Itoh, and T. Baba, IEEE J. Sel. Topics Quantum Electron. **1**, 473 (1995).
[15] G. P. Agrawal and N. K. Dutta, *Semiconductor Lasers* (Van Nostrand Reinhold, New York, 1993).
[16] V. W. L. Chin, T. L. Tansley, and T. Osotchan, J. Appl. Phys. **75**, 7365 (1994).
[17] A. S. Barker and M. Ilegems, Phys. Rev. B **7**, 743 (1973).
[18] J. W. Orton, Semicond. Sci. Technol. **10**, 101 (1995).
[19] S. Nakamura, Y. Harada, and M. Senoh, Appl. Phys. Lett. **58**, 2021 (1991).
[20] J. Edwards, K. Kawabe, G. Stevens, and R. H. Tredgold, Solid State Commun. **3**, 99 (1965).
[21] R. F. Davis, Physica B **185**, 1 (1993).
[22] H. Morkoc, S. Strite, G. B. Gao, M. E. Lin, B. Sverdlov, and M. Burns, J. Appl. Phys. **76**, 1363 (1994).
[23] H. Yamashita, K. Fukui, S. Misawa, and S. Yoshida, J. Appl. Phys. **50**, 896 (1979).
[24] S. Logothetidis, J. Petalas, M. Cardona, and T. D. Moustakas, Phys. Rev. B **50**, 18017 (1994).
[25] W. A. Harrison, *Electronic Structure and the Properties of Solids: The Physics of the Chemical Bond* (Freeman, San Francisco, 1980).
[26] C. M. Wolfe, N. Holonyak, Jr., and G. E. Stillman, *Physical Properties of Semiconductors* (Prentice-Hall, Englewood Cliffs, 1989).
[27] R. Dingle and M. Ilegems, Solid State Commun. **9**, 175 (1971).